



Preparation of $\text{ZnFe}_2\text{O}_4/\alpha\text{-Fe}_2\text{O}_3$ Nanocomposites From Sulfuric Acid Leaching Liquor of Jarosite Residue and Their Application in Lithium-Ion Batteries

Jinhuan Yao, Jing Yan, Yu Huang, Yanwei Li*, Shunhua Xiao and Jianrong Xiao*

Guangxi Key Laboratory of Electrochemical and Magneto-Chemical Functional Materials, College of Chemistry and Bioengineering, Guilin University of Technology, Guilin, China

OPEN ACCESS

Edited by:

Qiaobao Zhang,
Xiamen University, China

Reviewed by:

Ting-Feng Yi,
Northeast University at Qinhuangdao
Campus, China
Xiao-Dong Zhu,
Harbin Institute of Technology, China
Lingjun Li,
Changsha University of Science and
Technology, China

*Correspondence:

Yanwei Li
lywhit@126.com
Jianrong Xiao
xjr@glut.edu.cn

Specialty section:

This article was submitted to
Physical Chemistry and Chemical
Physics,
a section of the journal
Frontiers in Chemistry

Received: 10 July 2018

Accepted: 05 September 2018

Published: 25 September 2018

Citation:

Yao J, Yan J, Huang Y, Li Y, Xiao S and
Xiao J (2018) Preparation of
 $\text{ZnFe}_2\text{O}_4/\alpha\text{-Fe}_2\text{O}_3$ Nanocomposites
From Sulfuric Acid Leaching Liquor of
Jarosite Residue and Their Application
in Lithium-Ion Batteries.
Front. Chem. 6:442.
doi: 10.3389/fchem.2018.00442

Recycling Zn and Fe from jarosite residue to produce high value-added products is of great importance to the healthy and sustainable development of zinc industry. In this work, we reported the preparation of $\text{ZnFe}_2\text{O}_4/\alpha\text{-Fe}_2\text{O}_3$ nanocomposites from the leaching liquor of jarosite residue by a facile chemical coprecipitation method followed by heat treatment at 800°C in air. The microstructure of the as-prepared $\text{ZnFe}_2\text{O}_4/\alpha\text{-Fe}_2\text{O}_3$ nanocomposites were characterized by X-ray diffraction (XRD), Mössbauer spectroscopy, scanning transmission electron microscope (STEM), and X-ray photoelectron spectrum (XPS). The results demonstrated that the $\text{ZnFe}_2\text{O}_4/\alpha\text{-Fe}_2\text{O}_3$ composites are composed of interconnected ZnFe_2O_4 and $\alpha\text{-Fe}_2\text{O}_3$ nanocrystals with sizes in the range of 20–40 nm. When evaluated as anode material for Li-ion batteries, the $\text{ZnFe}_2\text{O}_4/\alpha\text{-Fe}_2\text{O}_3$ nanocomposites exhibits high lithium storage activity, superior cyclic stability, and good high rate capability. Cyclic voltammetry analysis reveals that surface pseudocapacitive lithium storage has a significant contribution to the total stored charge of the $\text{ZnFe}_2\text{O}_4/\alpha\text{-Fe}_2\text{O}_3$, which accounts for the enhanced lithium storage performance during cycling. The synthesis of $\text{ZnFe}_2\text{O}_4/\alpha\text{-Fe}_2\text{O}_3$ nanocomposites from the leaching liquor of jarosite residue and its successful application in lithium-ion batteries open up new avenues in the fields of healthy and sustainable development of industries.

Keywords: lithium-ion batteries, $\text{ZnFe}_2\text{O}_4/\alpha\text{-Fe}_2\text{O}_3$ composites, anode materials, jarosite residue, chemical coprecipitation method

INTRODUCTION

As one of the most promising energy storage systems, rechargeable lithium-ion batteries (LIBs) have been widely applied in portable electronic devices, electric vehicles, and smart grids (Dunn et al., 2011; Scrosati et al., 2011; Larcher and Tarascon, 2014). To meet the ever-increasing requirements of high power density and high energy density, developing new electrode materials with high specific capacity and high rate capability is very crucial for manufacturing the next-generation LIBs (Tang et al., 2015; Yi et al., 2016; Zhu and Yi, 2016; Massé et al., 2017; Yao et al., 2018a). The commercial graphite anode material for LIBs suffers from low theoretical capacity (about 372 mAh g⁻¹), poor rate performance, and serious safety issues,

and therefore cannot fulfill demands for LIBs with high energy density, high power density, and good safety in operation (Goriparti et al., 2014; Yi et al., 2015; Zhang et al., 2018). Over recent years, transition metal oxides (TMOs) have attracted extensive attention for their high theoretical specific capacities (600–1,200 mAh g⁻¹) and good safety as anode materials for LIBs (Reddy et al., 2013; Nitta and Yushin, 2014; Yuan et al., 2014; Pan et al., 2015b; Zhu et al., 2015). Among the various TMOs, Fe-based oxides have been widely studied due to their abundance, low cost, safety, wide availability, and environmental friendliness (Zhang et al., 2014; Pan et al., 2015a; Xu et al., 2015; Yao et al., 2018c; Zheng Z. M. et al., 2018). In particular, ZnFe₂O₄ and Fe₂O₃ stand out from the Fe-based oxides because of their high theoretical capacities (1,072 mAh g⁻¹ for ZnFe₂O₄ and 1,007 mAh g⁻¹ for Fe₂O₃). However, the poor power capability, and fast capacity fading owing to the huge volume changes during discharge/charge cycles for ZnFe₂O₄ and Fe₂O₃, severely hinders their practical applications in LIBs (Reddy et al., 2013; Zhang S. L. et al., 2017; Yao et al., 2018b). Constructing appropriate nanostructures has been demonstrated to be an effective way to improve the electrochemical performance of electrode active materials (Zhang et al., 2013; Yu et al., 2018). Various nanostructured ZnFe₂O₄ and Fe₂O₃ materials have been fabricated using diverse methods, such as sol-gel method (Thankachan et al., 2015), hydrothermal synthesis (Lin and Pan, 2015; Li L. L. et al., 2017; Zheng Z. M. et al., 2018), solvothermal synthesis (Lu et al., 2013; Yang et al., 2017), high energy ball-milling, electrospinning method (Wang C. L. et al., 2017), and reactive pulsed laser deposition method (NuLi et al., 2004). Although improved electrochemical performances have been achieved, most of the reported methods are generally time-consuming and involving complicated steps, high cost due to high energy consumption and expensive raw materials, and difficult to scale up, which greatly restrict the development and practical application of nanostructured ZnFe₂O₄ and Fe₂O₃ materials in LIBs. Therefore, it is still a big challenge but urgent demand to pursue a facile, efficient, and inexpensive method for massive production of nanostructured Fe-based oxide electrode materials with high performance for next-generation LIBs. Recycling waste materials can ease the resource crisis, reduce environmental pollution, and create new economic values, which has a great practical significance for the healthy and sustainable improvement of the human living environment. Huge quantities of jarosite residue was produced from traditional zinc hydrometallurgy process in the world. Most of the jarosite residue was stored up, which takes massive land and brings forth great risk of environmental pollution (Ju et al., 2011). The leaching liquor (containing Zn and Fe) of jarosite residue can be directly used to prepare high value-added Fe-based oxides functional materials, which has not been reported until now.

Herein, we reported the use of leaching liquor of jarosite residue to prepare ZnFe₂O₄/α-Fe₂O₃ nanocomposites by a chemical coprecipitation method followed by heat treatment at 800°C in air. This method offers the merits of low-cost, facile, and scalable production of nanostructured ZnFe₂O₄/α-Fe₂O₃ composites. When studied as anode materials for LIBs, the as-prepared porous ZnFe₂O₄/α-Fe₂O₃ nanocomposites exhibit

high reversible capacity, excellent cycling stability and good high rate capability, which can be attributed to the synergetic effect between ZnFe₂O₄ and α-Fe₂O₃ nanoparticles and the significant pseudocapacitive behavior during discharging and charging processes.

EXPERIMENTAL

Preparation of ZnFe₂O₄/α-Fe₂O₃ Nanocomposites

All chemicals employed in this work were of analytical reagent grade and used without further purification. The leaching liquor contains 44 mM Zn²⁺, 121 mM Fe²⁺, and a small amount of Cu²⁺, Ca²⁺, As³⁺, and In³⁺. In a typical procedure, 0.464 g ZnSO₄·7H₂O was dissolved in 100 mL leaching liquor so that the molar ratio of Zn²⁺ and Fe³⁺ in the solution is 1:2. After ultrasonic treatment for 10 min, an aqueous solution of NH₄OH (200 mL, ~2.67 M) was added dropwise into the above mixed solution under constant vigorous stirring at room temperature. After continuous stirring for 3 h, the deposit was kept in the mother solution at room temperature for 12 h and allowed to settle, then washed with deionized water, filtered, and dried in an oven at 80°C overnight to get the precursor. Finally, the as-prepared precursor was calcinated at 800°C for 2 h in air to obtain the ZnFe₂O₄/α-Fe₂O₃ sample.

Physical Characterization

The crystal structure of the as-prepared sample was identified with a powder X-ray diffractometer (XRD, Dutch PANalytica X'Pert³ powder) with Cu Kα radiation (λ = 1.5406 Å). The X-ray tube voltage and current were set at 40 kV and 40 mA, respectively. Field-emission scanning electron microscope (FESEM, Hitachi SU500) and transmission electron microscope (HRTEM, JEM-2100F) were used to analyze the microstructure of the as-prepared sample. ⁵⁷Fe Mössbauer spectrum was recorded by using an MFD-500A Mössbauer spectrometer (Topologic Systems, Japan). To determine the surface composition and chemical states of the sample, X-ray photoelectron spectroscopy (XPS) analysis was carried out using an ESCALAB 250 spectrometer (Perkin-Elmer), with an Al Kα source (1486.6 eV) operated at 15 kV and 150 W, at a base pressure of 2 × 10⁻⁹ Torr.

Electrochemical Measurements

The electrochemical performance of the ZnFe₂O₄/α-Fe₂O₃ nanocomposites was evaluated in CR2032-type coin cells assembled in an argon-filled glovebox. The test electrodes were fabricated by mixing active materials (ZnFe₂O₄/α-Fe₂O₃ nanocomposites), Super-P carbon black, and binder (polyvinylidene difluoride, PVDF) with a weight ratio of 6:3:1 in N-methyl-2-pyrrolidone (NMP) solvent. The obtained slurry was uniformly coated onto a copper foil and then dried under at 80°C for 12 h in a vacuum oven. The mass loading of the working electrode is ~1.0 mg cm⁻¹. Metallic lithium foils were used as both the counter and reference electrodes. A Celgard 2400 microporous polypropylene membrane was used as the separator. The electrolyte was 1M LiPF₆ solution, composing of

ethylene carbonate (EC), diethyl-carbonate (DEC), and dimethyl carbonate (DMC) (1:1:1, in volume). Cyclic voltammetry (CV) and electrochemical impedance spectroscopy (EIS) profiles were carried out on a CHI760E electrochemical workstation. The CVs were recorded within the potential range of 0.01–3.0 V (vs. Li/Li⁺) at various of scanning rates. The EIS spectra were measured in the frequency ranging from 100 mHz to 100 kHz by applying an AC amplitude of 5 mV at a fully charged state. The galvanostatic discharge/charge measurements were performed on a NEWARE battery testing system in the voltage range

of 0.01–3.0 V (vs. Li/Li⁺). All the electrochemical tests were performed at room temperature.

RESULTS AND DISCUSSION

Structure Characterization

Figure 1 shows XRD pattern of the as-prepared ZnFe₂O₄/α-Fe₂O₃ nanocomposites. The diffraction peaks of the nanocomposites can be well indexed to either rhombohedra α-Fe₂O₃ (JCPDS 87-1164) or spinel ZnFe₂O₄ (JCPDS 82-1049).

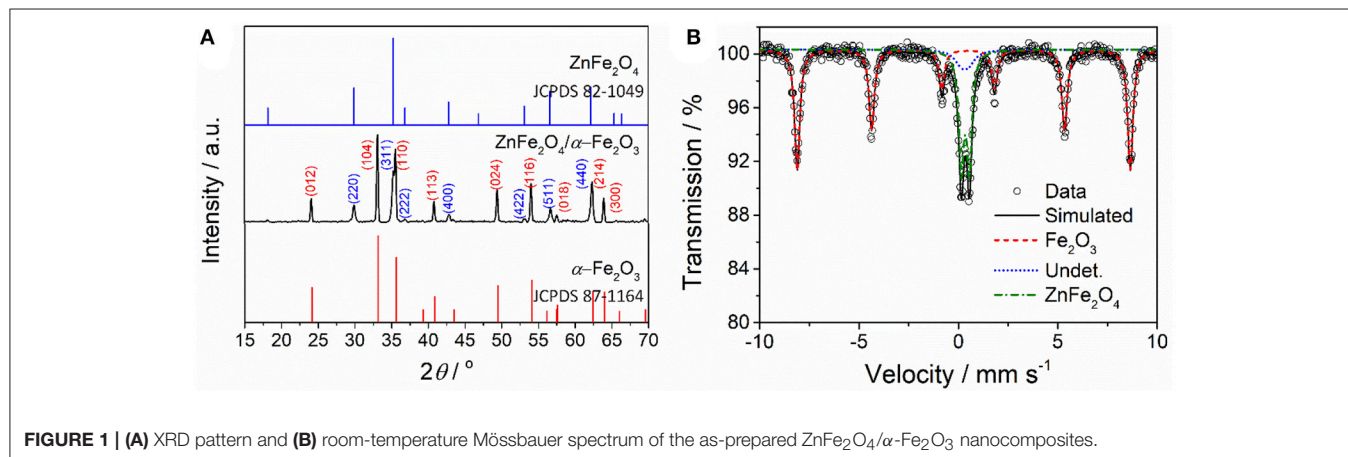


FIGURE 1 | (A) XRD pattern and (B) room-temperature Mössbauer spectrum of the as-prepared ZnFe₂O₄/α-Fe₂O₃ nanocomposites.

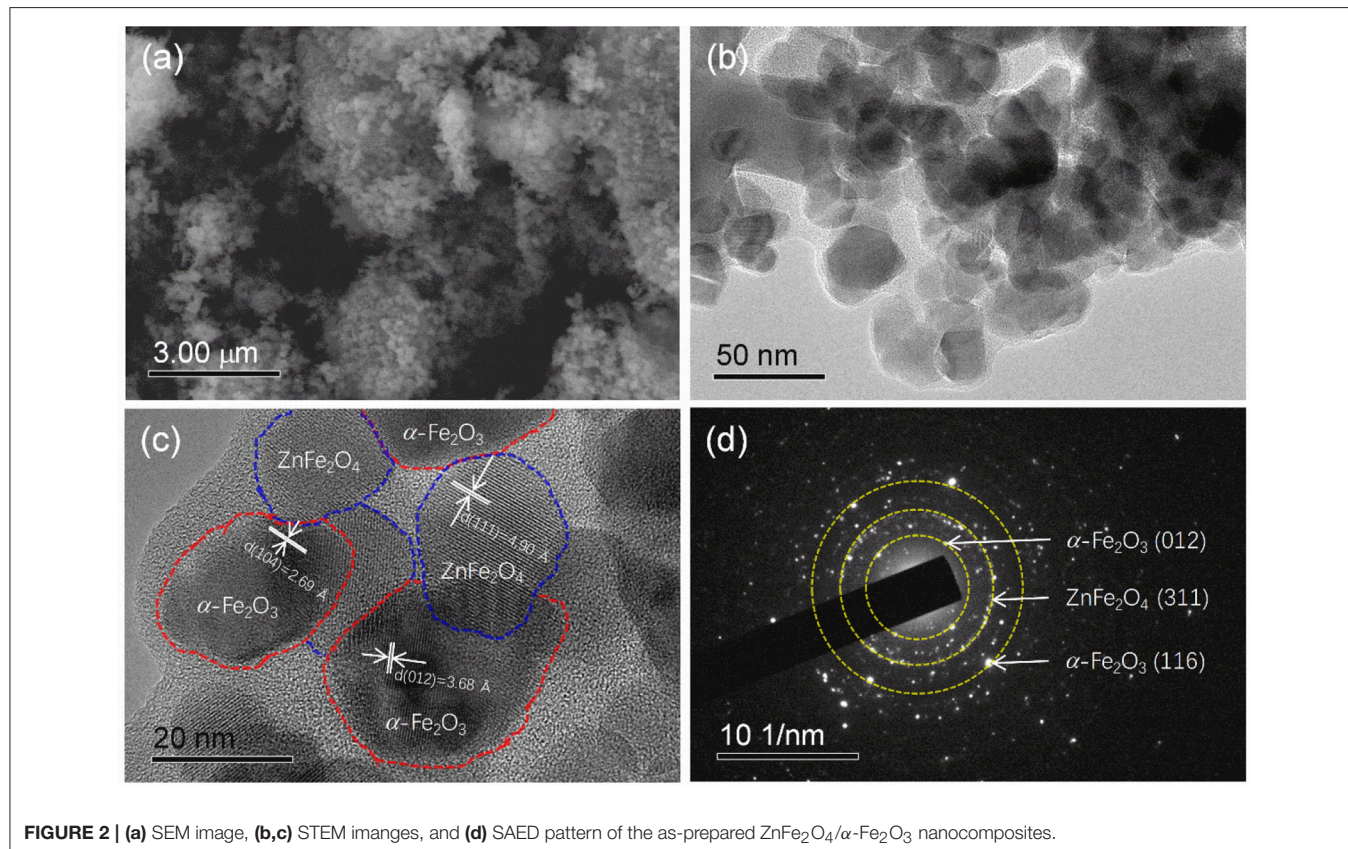


FIGURE 2 | (a) SEM image, (b,c) STEM images, and (d) SAED pattern of the as-prepared ZnFe₂O₄/α-Fe₂O₃ nanocomposites.

No diffraction peaks from impurities are detected, suggesting the nanocomposites are composed of spinel ZnFe₂O₄ phase and α-Fe₂O₃ phase. The average crystal sizes of the ZnFe₂O₄ phase and α-Fe₂O₃ phase in the nanocomposites estimated using Scherrer's formula are about 30 and 44 nm, respectively. ⁵⁷Fe Mössbauer spectroscopy was used to determine the phase composition and metal cation redistribution in the ZnFe₂O₄/α-Fe₂O₃ nanocomposites and the result is presented in **Figure 2b**. The dots in **Figure 2b** are experimental spectrum and the continuous curves are fitting lines. **Table 1** summarizes the Mössbauer refined parameters from the fitting of the spectrum. The Mössbauer spectrum of the ZnFe₂O₄/α-Fe₂O₃ nanocomposites are fitted with one sextet and two doublets. The sextet can be assigned to α-Fe₂O₃ with iron content 63% in the composites (Pailhé et al., 2008; Lazarević et al., 2014), and the doublets can be due to super paramagnetic ZnFe₂O₄ with iron content 37% in the composites (Yao et al., 2012; Amir et al., 2018). The doublet with a lower quadrupole splitting can

be assigned to the Fe³⁺ at tetrahedral sites in ZnFe₂O₄ (Amir et al., 2018). The site occupation in ZnFe₂O₄ can be represented by (Zn_{1-λ}Fe_λ)_{tet}[Zn_λFe_{2-λ}]_{oct}O₄ where λ is the inversion parameter (0 ≤ λ ≤ 1). The calculated inversion parameter of the ZnFe₂O₄ phase is 0.22. Thus, the chemical formula of the ZnFe₂O₄ phase in the nanocomposites can be expressed as (Zn_{0.78}Fe_{0.22})[Zn_{0.22}Fe_{1.78}]O₄.

Figure 2a presents the SEM image of the as-prepared ZnFe₂O₄/α-Fe₂O₃ nanocomposites. It can be seen that the sample is composed of agglomerated nanosized primary particles. More detail structure information about the ZnFe₂O₄/α-Fe₂O₃ nanocomposites was obtained from STEM analyses. The low- and high-magnification STEM images (**Figures 2b,c**) show that the ZnFe₂O₄/α-Fe₂O₃ nanocomposites are actually composed of interconnected nanocrystals with size in the range of 20~50 nm, which is consistent with the result from the XRD analysis. The ZnFe₂O₄ nanocrystals and α-Fe₂O₃ nanocrystals could be well distinguished in the high-resolution STEM image (**Figure 2c**). The selected area electron diffraction (SAED, **Figure 2d**) pattern of the ZnFe₂O₄/α-Fe₂O₃ nanocomposites suggests its polycrystalline character and the distinct diffraction spots could be assigned sequentially to α-Fe₂O₃ (012), ZnFe₂O₄ (311), and α-Fe₂O₃ (116) planes from the center, which also appear in the XRD pattern (**Figure 1A**). The primary nanocrystals of the ZnFe₂O₄/α-Fe₂O₃ nanocomposites offer large surface area and short diffusion pathways for fast Li⁺ diffusion; the interconnected primary nanocrystals provide

TABLE 1 | Mössbauer parameters for the ZnFe₂O₄/α-Fe₂O₃ nanocomposites.

Fitting lines	Assignment of sites	IS (mm s ⁻¹)	QS (mm s ⁻¹)	R _A (%)
Sextet	Fe ₂ O ₃	0.376	-0.220	63.2
Doublet	Fe ³⁺ (A) _{tet}	0.319	0.384	7.6
Doublet	Fe ³⁺ (B) _{oct}	0.348	0.406	29.2

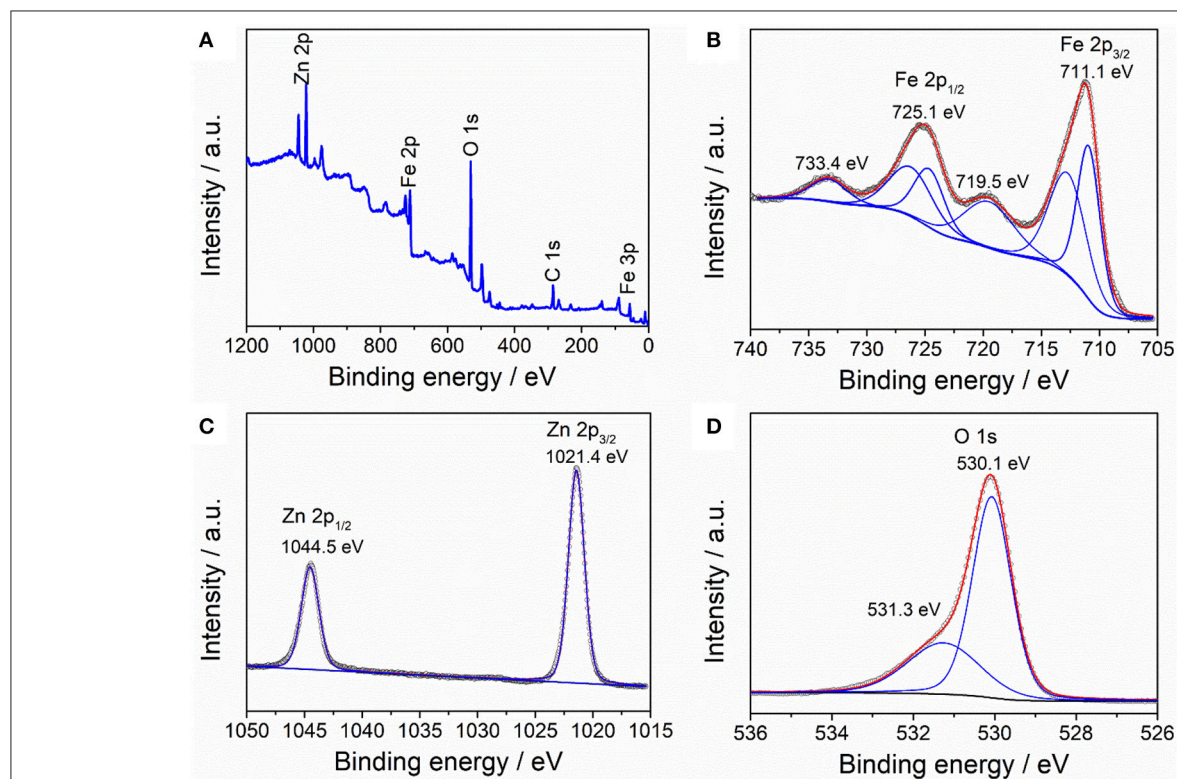
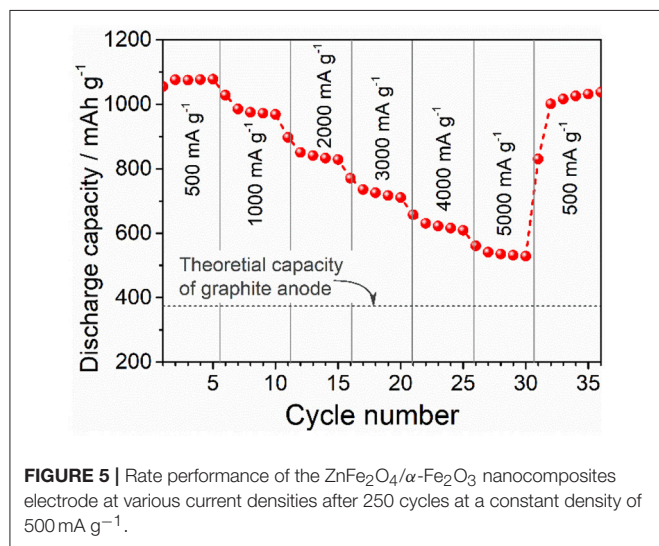
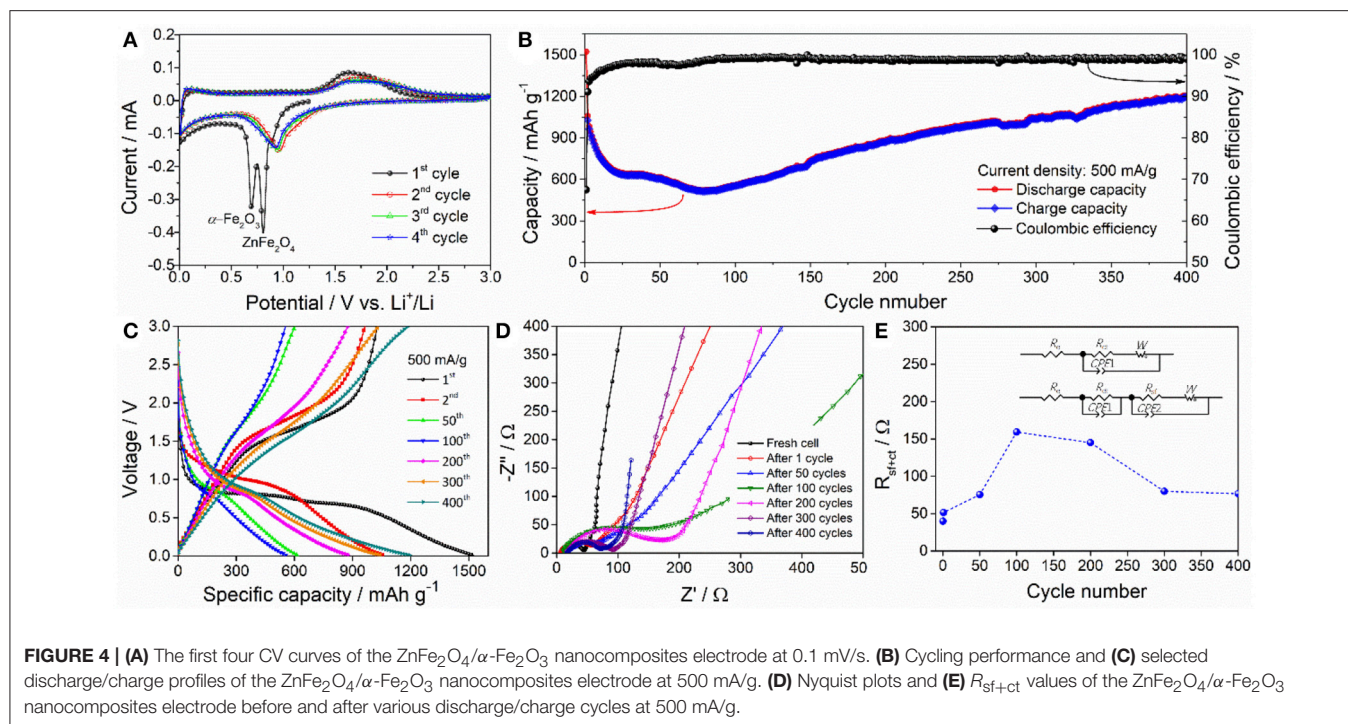


FIGURE 3 | XPS spectra of ZnFe₂O₄/α-Fe₂O₃ nanocomposites: **(A)** survey of the sample, **(B)** Fe 2p, **(C)** Zn 2p, and **(D)** O 1s.



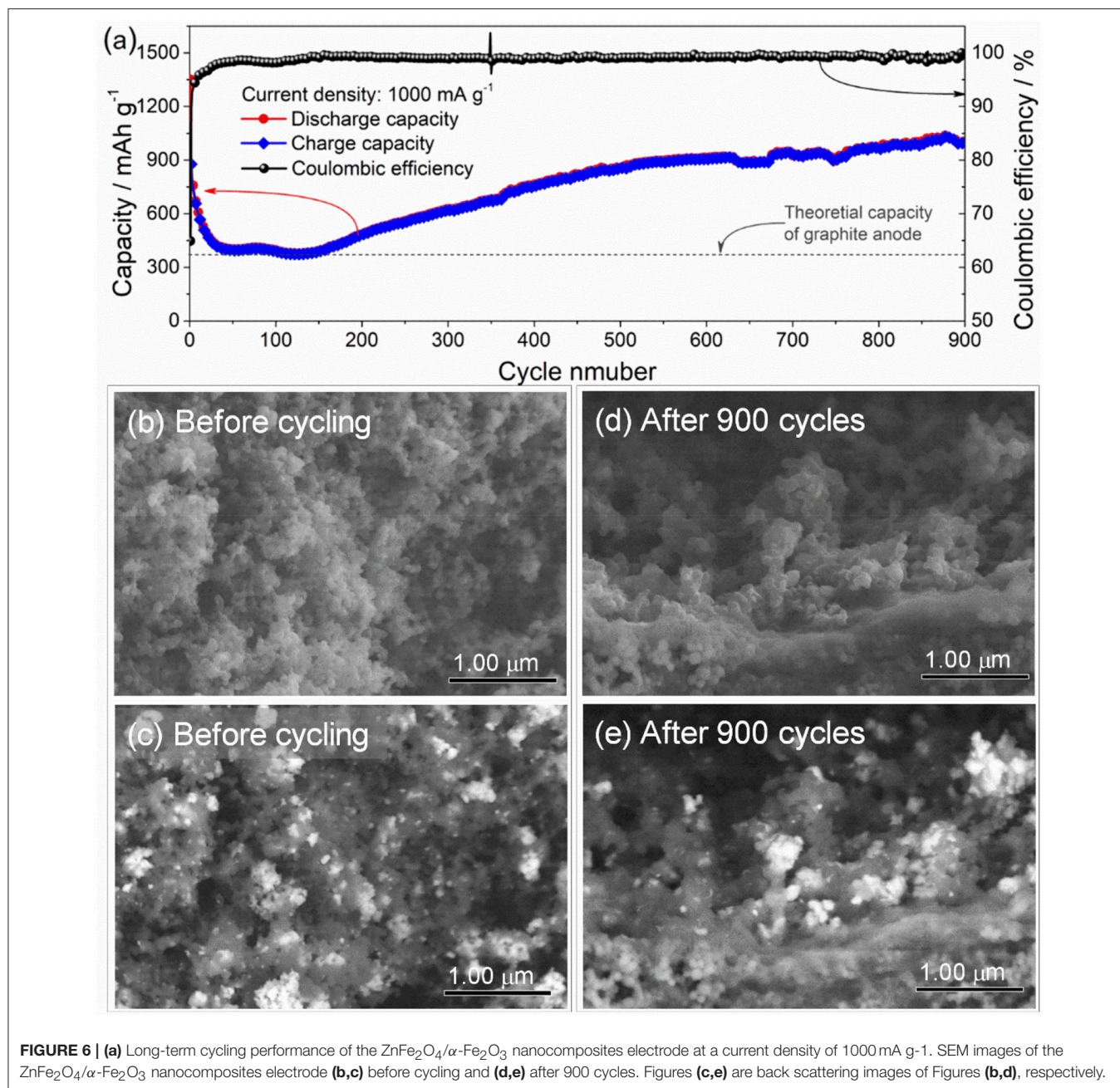
continuous electronic transfer channels in the ZnFe₂O₄/ α -Fe₂O₃ composites; the large amount of void spaces among the interconnected nanocrystals would benefit the penetration of electrolyte in electrode, and accommodate the strain induced by the volume change upon discharge/charge cycling. Moreover, the interconnected ZnFe₂O₄/ α -Fe₂O₃ heterojunctions could provide an enhanced inner electric field at the interface between ZnFe₂O₄ and α -Fe₂O₃ nanocrystals, which will greatly accelerate the charge-transfer kinetics during electrochemical reactions (Qiao et al., 2013; Zhao et al., 2014; Zheng et al., 2016).

The composition and element valence of the as-prepared ZnFe₂O₄/ α -Fe₂O₃ nanocomposites were characterized by XPS and the result are displayed in Figure 3. The survey XPS spectrum (Figure 3A) shows the presence of elements Zn, Fe, and O, as well as C, which comes from the adsorbed CO₂ and/or hydrocarbon contaminations.

The Fe 2p core peak spectrum shows two main peaks at 711.1 and 725.1 eV, which can be assigned to Fe_{3/2} and Fe_{1/2}, respectively (Guo et al., 2014). The presence of two satellite peaks at 719.5 and 733.4 eV is characteristic of the Fe³⁺ in the ZnFe₂O₄/ α -Fe₂O₃ nanocomposites (Zhao et al., 2014). The Zn 2p core peak spectrum is composed of two intense peaks at 1021.4 and 1044.5 eV, which can be ascribed to Zn 2p_{3/2} and Zn 2p_{1/2} of Zn²⁺, respectively (Lu et al., 2017). The O 1s core peak spectrum consists of two peaks at 530.1 and 531.3 eV, which can be attributed to the lattice oxygen in the nanocomposites and surface-adsorbed hydrocarbon (Zhang L. H. et al., 2017).

Electrochemical Characterization

Figure 4A displays the typical CV profiles of ZnFe₂O₄/ α -Fe₂O₃ nanocomposites electrode for the first four cycles between 0.01 and 3.0 V at a scan rate of 0.1 mV/s. During the first cycle, two intense reduction peaks can be observed at about 0.70 and 0.81 V, which can be associated with the initial reduction of ZnFe₂O₄ to metallic Fe⁰/Zn⁰ and the complete reduction of α -Fe₂O₃ to metallic Fe⁰, as well as the formation of amorphous Li₂O matrix and solid electrolyte interface (SEI) film (Zhang Y. M. et al., 2017); the broad oxidation peak at about 1.63 V can be attributed to the oxidation of the metallic Zn⁰ and Fe⁰ to Zn²⁺ and Fe³⁺, respectively (Yao et al., 2018c). In the subsequent cycles, the two reduction peaks merges together and

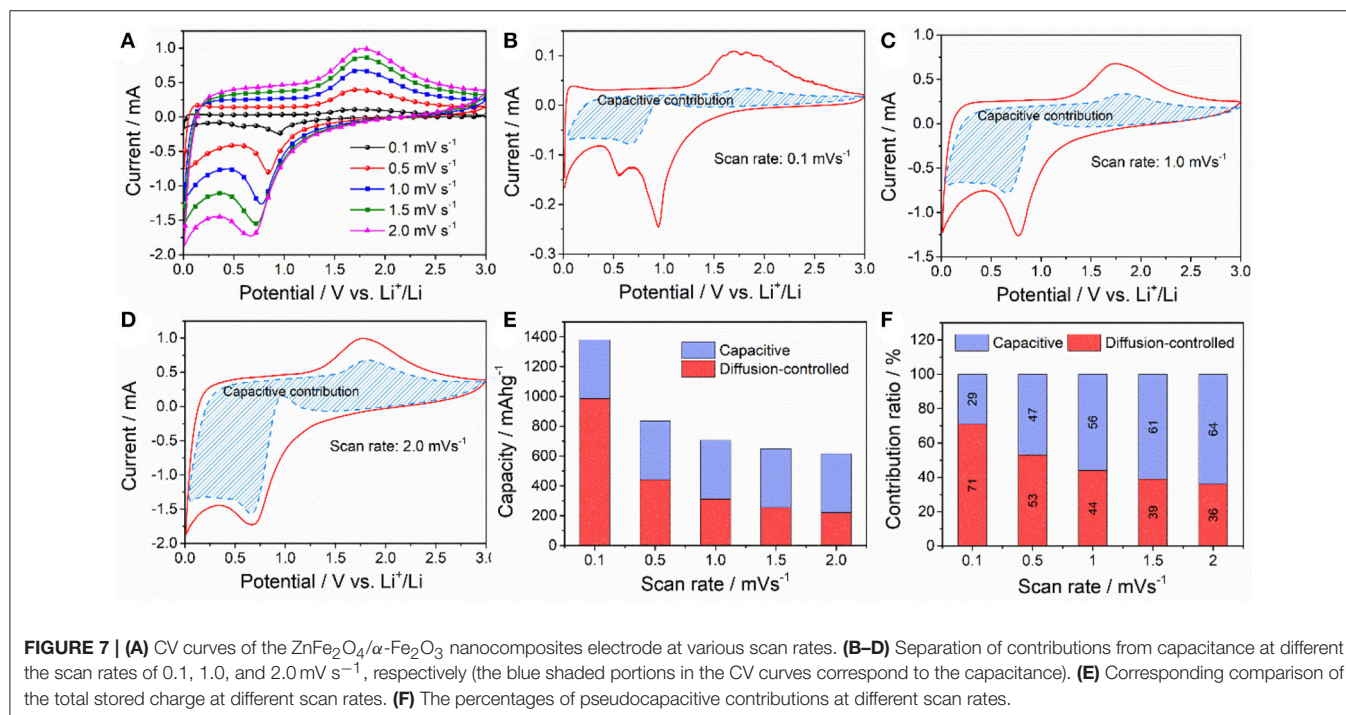


shifts to 0.97 V, which can be due to the drastic lithium-driven structural and/or textural modifications on the electrode during the first lithiation process; the oxidation peak slightly shifts to 1.69 V, which can be ascribed to structure rearrangement after the first lithiation/delithiation process (Zhang Y. M. et al., 2017; Zhou et al., 2017). The well-overlapped CV profiles of the third and the fourth cycle suggest the good electrochemical reaction reversibility of the nanocomposites electrode. **Figure 4B** gives the cycling performance of the ZnFe₂O₄/α-Fe₂O₃ nanocomposites electrode at a current density of 500 mA g⁻¹. The initial discharge and charge capacities are 1,522 and 1,027 mAh g⁻¹, with a coulombic efficiency of 67.5%. This large irreversible capacity loss

during the first cycles is mainly caused by the irreversible reaction and formation of the SEI layer on the surface of electroactive materials (Reddy et al., 2013). The electrode exhibits a rapid capacity decay in the first 20 cycles and relatively slow capacity decay from the 20 to 80th cycle, which can be ascribed to the mechanical degradation and unstable SEI formation upon discharge/charge cycling (Sun et al., 2014). After 80 cycles, the discharge capacity increases gradually and gets 1,206 mAh g⁻¹ in the 400th cycle. The rise of the discharge capacity may result from the synergistic combination of the refinement of nanoparticles and the formation of organic polymeric/gel-like layer by electrolyte decomposition with the increase of the

TABLE 2 | Comparison of lithium storage performance of ZnFe₂O₄-based nanomaterials from previous work and this work.

Samples	Current density (mA g ⁻¹)	Discharge capacity (mAh g ⁻¹)	References
ZnFe ₂ O ₄ /carbon nanocomposites	200	1,090 after 400 cycles	Jiang et al., 2016
Mesoporous ZnFe ₂ O ₄ /graphene composites	1,000	870 after 100 cycles	Yao et al., 2014c
Nano sized ZnFe ₂ O ₄ /flake graphene composites	100	730 after 100 cycles	Yao et al., 2014a
Mesoporous ZnFe ₂ O ₄ /C composite microspheres	50	1,100 after 100 cycles	Yao et al., 2014b
ZnFe ₂ O ₄ /carbon nanodiscs	100	965 after 100 cycles	Jin et al., 2015
ZnFe ₂ O ₄ /γ-Fe ₂ O ₃ nanoparticles	500	360 after 300 cycles	Bourrioux et al., 2017
ZnFe ₂ O ₄ nanospheres/graphene composites	1,000	704 after 50 cycles	Shi et al., 2015
Nitrogen-doped carbon coated ZnFe ₂ O ₄	1,000	700 after 1,000 cycles	Yue et al., 2015
ZnFe ₂ O ₄ /C hollow spheres	65	841 after 30 cycles	Deng et al., 2011
ZnFe ₂ O ₄ nano-octahedrons	1,000	730 after 300 cycles	Xing et al., 2012
ZnFe ₂ O ₄ /α-Fe ₂ O ₃	1,000	1,000 after 900 cycles	This work



number of cycles (Hassan et al., 2011; Rai et al., 2014; Wang M. Y. et al., 2017). **Figure 4C** presents the typical discharge/charge curves of the nanocomposites electrode in different cycles at a current density of 500 mA g⁻¹. After the first discharge/charge cycle, the long discharge plateau change into a slope. The change of the voltage plateaus and the large capacity loss after the first cycle match well with the CV profiles (**Figure 4A**). Moreover, the voltage hysteresis between discharge and charge profiles enlarges in the first 100 cycles, and then reduces gradually, implying that the electrode state and polarization degree vary with discharge/charge cycles. **Figure 4D** displays the Nyquist plots of the nanocomposites electrodes recorded before cycling and after selected discharge/charge cycles. Each plot consists of one depressed semicircle or two semicircles in the high to moderate frequency region and an inclined line in the low

frequency region. The depressed semicircles can be assigned to the resistance of Li⁺ migrating through the SEI film and the charge-transfer resistance at electrode/electrolyte interface (denoted as R_{sf+ct}), and the inclined line represents the Warburg impedance related to Li⁺ diffusion process into the bulk of the electrode (Wang et al., 2015; Li et al., 2016; Kong et al., 2017; Lee et al., 2017). Before cycling, the Warburg straight line is almost vertical to the real-axis (capacitive behavior), suggesting that there is almost no detectable Li⁺ intercalation in the electrode for fresh cell. With the number of cycles increasing from 1 to 100, the Warburg straight line gradually decreases to an angle of ~45° to the real-axis, showing the characteristic of Li⁺ diffusion in the electrode; however, further increasing the number of cycles from 100 to 400, the Warburg straight line gets more and more steep, presenting the characteristic of pseudocapacitive behavior,

which may derive from the reversible formation of organic polymeric/gel-like layer (Laruelle et al., 2002). The Nyquist plots were fitted by the equivalent circuits shown as inset in **Figure 4E**. In the circuits, the R_e , R_{sf} , and R_{ct} are electrolyte resistance, SEI layer resistance, and charge transfer resistance, respectively. $CPE1$ and $CPE2$ are the corresponding capacitances of R_{sf} and R_{ct} . W is the Warburg impedance. The calculated R_{sf+ct} values of the electrodes before and after different discharge/charge circles is presented in **Figure 4E**. Before cycling, the R_{sf+ct} value of the electrode is 40 Ω. During the initial 100 cycles, the R_{sf+ct} value increases from 51 to 195 Ω; further increasing the number of cycles increase from 100 cycles to 300 and 400 cycles, the R_{sf+ct} value decreases from 195 to 80 and 77 Ω, respectively. The EIS results reveals that the decrease in capacity during the initial 80 cycles can be due to the slow Li⁺ diffusion process and large resistances from SEI film and charge-transfer process (high polarization); the increasing capacity in the following cycles from 80 to 400 cycles can be explained by the enhanced Li⁺ diffusion process and reduced resistances from SEI film and charge-transfer process (low polarization).

The rate performance of the of ZnFe₂O₄/α-Fe₂O₃ nanocomposites electrode was tested after the electrode is activated at 500 mA g⁻¹ for 250 cycles, and the result are shown in **Figure 5**. With the increase of current density, the discharge capacity decreases gradually. Even at the very high current density of 5,000 mA g⁻¹, the specific capacity (535 mAh g⁻¹) still obviously higher than the theoretical capacity (372 mAh g⁻¹) of graphite. When the current density reverses back to 500 mA g⁻¹, the discharge capacity almost recovers to the original values, implying the good capacity retention performance of the electrode.

Figure 6a gives long-term cycling performance of the ZnFe₂O₄/α-Fe₂O₃ nanocomposites electrode at current density of 1,000 mA g⁻¹ for 900 cycles. It can be seen that the electrode exhibits excellent long-term cycling performance with a high capacity of about 1,000 mAh g⁻¹ after 900 cycles at the constant current density of 1,000 mA g⁻¹. Compared with previous work, the as-prepared ZnFe₂O₄/α-Fe₂O₃ nanocomposites deliver better electrochemical performance in terms of reversible discharge capacities and cycling stability (**Table 2**). **Figures 6b–e** presents the SEM images of the ZnFe₂O₄/α-Fe₂O₃ nanocomposites electrode before and after 900 cycles. To identify ZnFe₂O₄/α-Fe₂O₃ nanocomposites more clearly in the electrode, backscattered electron images are also provided. It can be seen that the as-prepared electrode shows the presence of ZnFe₂O₄/α-Fe₂O₃ nanocomposites constructed by interconnected primary nanocrystals before cycling (**Figures 6b,c**). After 900 cycles, the electrodes almost maintains the original morphology (**Figures 6b,c**); the ZnFe₂O₄/α-Fe₂O₃ nanocomposites can be clearly observed in the electrode and the nanocrystals are well interconnected with each other, implying the ZnFe₂O₄/α-Fe₂O₃ nanocomposites are flexible to alleviate volume expansion upon repeated discharge/charge cycles.

To better understand the superior lithium storage performance of the ZnFe₂O₄/α-Fe₂O₃ nanocomposites, we analyze the charge storage mechanism by the sweep voltammetry method proposed by Dunn et al. (Qu et al., 2017). In this

method, the contributions from capacitive effect and diffusion-controlled Li⁺ process can be quantified by the following equations:

$$i(V) = k_1 v + k_2 v^{1/2} \quad (1)$$

$$i(V)/v^{1/2} = k_1 v^{1/2} + k_2 \quad (2)$$

where $I(V)$ and v represent the total current response at a given potential V and scan rate for the CV measurements; $k_1 v$ and $k_2 v^{1/2}$ represent the current due to surface capacitive effects and current due to diffusion-controlled reaction process, respectively. By determining k_1 and k_2 , the currents arising from capacitive effect and diffusion-controlled Li⁺ process can be distinguished. **Figure 7A** gives the series of CV curves of ZnFe₂O₄/α-Fe₂O₃ nanocomposites electrode recorded at different scan rate. **Figures 7B–D** illustrate the typical voltage profiles for the capacitive current (blue shaded region) in comparison with the total current obtained at the scan rate of 0.1, 1.0, and 2.0 mV s⁻¹, respectively. Obviously, capacitive charge storage contributes a significant proportion to the total capacity, in particular in the low potential region (0.8–0.01 V) during delithiation process. With the increase of scan rate, the portion from capacitive capacity increases dramatically. As shown in **Figure 7E**, the capacitive capacity makes up about 29% of the total capacity at the scan rate of 0.1 mV s⁻¹, whereas this value increases to 56% and 64% at the scan rate of 1 and 2 mV s⁻¹, respectively. Similar results have also been reported for the nano-sized NiO and Ni(OH)₂ anode materials (Li Y. W. et al., 2017b; Zheng Y. Y. et al., 2018). This significant surface or near surface charge storage due to capacitive behavior benefits the high rate capability and cycling stability of electrode active materials (Rauda et al., 2013; Augustyn et al., 2014; Li Y. W. et al., 2017a).

The superior lithium storage performance of the ZnFe₂O₄/α-Fe₂O₃ nanocomposites can be ascribed to following several aspects: (1) the primary nanocrystals facilitate the transport of both Li⁺ and electrons because of the short diffusion distance, which enhances the kinetic performance; (2) the numerous void spaces among the interconnected primary nanoparticles and among the nanoparticles can accommodate the strain induced by the volume change during discharge/charge cycles, and therefore improve the cycling performance; (3) the unique ZnFe₂O₄/α-Fe₂O₃ heterojunctions provides an enhanced inner electric field at the interface between ZnFe₂O₄ and α-Fe₂O₃ nanocrystals, which may efficiently accelerate the charge-transfer kinetics during electrochemical reactions and boost the rate capability; (4) the significant pseudocapacitive behavior during discharge/charge process is also an important reason for the outstanding high rate capability and long-term cycling stability.

CONCLUSIONS

Hybrid ZnFe₂O₄/α-Fe₂O₃ nanocomposites have been successfully fabricated with the leaching liquor of jarosite residue as raw material by a facile chemical coprecipitation method followed by heat treatment in air. The ZnFe₂O₄/α-Fe₂O₃

nanocomposites are composed of interconnected ZnFe₂O₄ and α-Fe₂O₃ nanocrystals with sizes in the range of 20–40 nm. Due to the unique heterojunction nanostructure, the ZnFe₂O₄/α-Fe₂O₃ nanocomposites exhibits high lithium storage activity, superior cyclic stability, and good high rate capability when evaluated as anode materials for lithium-ion batteries. The reversible capacity of 1,000 mAh g⁻¹ is achieved over 900 cycles at the constant current density of 1,000 mA g⁻¹; even at the high current density of 5,000 mA g⁻¹, the specific discharge capacity of 535 mAh g⁻¹ can be obtained, which is still significantly higher than the theoretical capacity (372 mAh g⁻¹) of graphite. Charge storage mechanism analysis demonstrates that surface pseudocapacitive lithium storage has a significant contribution to the total stored charge of the ZnFe₂O₄/α-Fe₂O₃ nanocomposites, which accounts for the enhanced lithium storage performance during cycling. This work provides a facile, efficient, and low-cost method for the synthesis of high-performance Fe-based oxides anode materials by utilizing the leaching liquor of jarosite residue as raw material, which can make use of the industrial jarosite residue as resource, reduce the environment pollution, create

high value-added products, and will achieve both good social and economic benefits.

AUTHOR CONTRIBUTIONS

JinhY and YL conceived the idea. JingY prepared all materials and performed electrochemical characterizations. YH conducted SEM experiments. YL, JingY, JinhY, JX, and SX analyzed the data. JinhY and JingY wrote the manuscript. YL and JX commented on it. JinhY supervised the implementation of the project.

ACKNOWLEDGMENTS

The authors thank the financial supports from the National Natural Science Foundation of China (No. 51464009 and 51664012), Guangxi Natural Science Foundation of China (2017GXNSFAA198117 and 2015GXNSFGA139006), and Guangxi Key Laboratory of Electrochemical and Magnetochemical Functional Materials (EMFM20181102/EMFM20181117).

REFERENCES

- Amir, M., Gungunes, H., Baykal, A., Almessiere, M. A., Sözeri, H., Ercan, I., et al. (2018). Effect of annealing temperature on magnetic and mössbauer properties of ZnFe₂O₄ nanoparticles by sol-gel approach. *J. Supercond. Nov. Magn.* 15, 1–10. doi: 10.1007/s10948-018-4610-2
- Augustyn, V., Simon, P., and Dunn, B. (2014). Pseudocapacitive oxide materials for high-rate electrochemical energy storage. *Energy Environ. Sci.* 7, 1597–1614. doi: 10.1039/c3ee44164d
- Bourrioux, S., Wang, L. P., Rousseau, Y., Simon, P., Habert, A., Leconte, Y., et al. (2017). Evaluation of electrochemical performances of ZnFe₂O₄/γ-Fe₂O₃ nanoparticles prepared by laser pyrolysis. *New J. Chem.* 41, 9236–9243. doi: 10.1039/C7NJ00735C
- Deng, Y., Zhang, Q., Tang, S., Zhang, L., Deng, S., Shi, Z., et al. (2011). One-pot synthesis of ZnFe₂O₄/C hollow spheres as superior anode materials for lithium ion batteries. *Chem. Commun.* 47, 6828–6830. doi: 10.1039/c0cc05001f
- Dunn, B., Kamath, H., and Tarascon, J. M. (2011). Electrical energy storage for the grid: a battery of choices. *Science* 334, 928–935. doi: 10.1126/science.1212741
- Goriparti, S., Miele, E., Angelis, F. D., Fabrizio, E. D., Zaccaria, R. P., and Capiglia, C. (2014). Review on recent progress of nanostructured anode materials for Li-ion batteries. *J. Power Sources* 257, 421–443. doi: 10.1016/j.jpowsour.2013.11.103
- Guo, X., Zhu, H. J., Si, M. S., Jiang, C. J., Xue, D. S., Zhang, Z. H., et al. (2014). ZnFe₂O₄ nanotubes: microstructure and magnetic properties. *J. Phys. Chem. C* 118, 30145–30152. doi: 10.1021/jp507991e
- Hassan, M. F., Guo, Z., Chen, Z., and Liu, H. (2011). α-Fe₂O₃ as an anode material with capacity rise and high rate capability for lithium-ion batteries. *Mater. Res. Bull.* 46, 858–864. doi: 10.1016/j.materresbull.2011.02.011
- Jiang, B. B., Han, C. P., Li, B., He, Y. J., and Lin, Z. Q. (2016). *In-situ* crafting of ZnFe₂O₄ Nanoparticles impregnated within continuous carbon network as advanced anode materials. *ACS Nano* 10, 2728–2735. doi: 10.1021/acsnano.5b07806
- Jin, R. C., Liu, H., Guan, Y. S., Zhou, J. H., and Chen, G. (2015). ZnFe₂O₄/C nanodiscs as high performance anode material for lithium-ion batteries. *Mater. Lett.* 158, 218–221. doi: 10.1016/j.matlet.2015.06.030
- Ju, S., Zhang, Y., Zhang, Y., Xue, P., and Wang, Y. (2011). Clean hydrometallurgical route to recover zinc, silver, lead, copper, cadmium and iron from hazardous jarosite residues produced during zinc hydrometallurgy. *J. Hazard Mater.* 192, 554–558. doi: 10.1016/j.jhazmat.2011.05.049
- Kong, H., Lv, C., Yan, C., and Chen, G. (2017). Engineering mesoporous single crystals co-doped Fe₂O₃ for high-performance lithium ion batteries. *Inorg. Chem.* 56, 7642–7649. doi: 10.1021/acs.inorgchem.7b00008
- Larcher, D., and Tarascon, J. M. (2014). Towards greener and more sustainable batteries for electrical energy storage. *Nat. Chem.* 7, 19–29. doi: 10.1038/nchem.2085
- Laruelle, S., Grugeon, S., Poizat, P., Dollé, M., Dupont, L., and Tarascon, J. (2002). On the origin of the extra electrochemical capacity displayed by Mo/Li cells at low potential. *J. Electrochem. Soc.* 149, A627–A634. doi: 10.1149/1.1467947
- Lazarević, Z. Ž., Jovalekić, C., Ivanovski, V. N., Rečnik, A., Milutinović, A., Cekić, B., et al. (2014). Characterization of partially inverse spinel ZnFe₂O₄ with high saturation magnetization synthesized via soft mechanochemically assisted route. *J. Phys. Chem. Solids* 75, 869–877. doi: 10.1016/j.jpcc.2014.03.004
- Lee, D., Wu, M., Kim, D. K., Chae, C., Cho, M. K., Kim, J.-Y., et al. (2017). Understanding the critical role of the Ag nanophase in boosting the initial reversibility of transition metal oxide anodes for lithium-ion batteries. *ACS Appl. Mater. Interfaces* 9, 21715–21722. doi: 10.1021/acsami.7b01559
- Li, L. L., Jin, B., Dou, S. X., and Jiang, Q. (2017). Facile fabrication of ZnFe₂O₄-MWCNTs composite as an anode material for rechargeable lithium-ion batteries. *Chemistryselect* 2, 7194–7201. doi: 10.1002/slct.201701206
- Li, Y. W., Pan, G. L., Xu, W. Q., Yao, J. H., and Zhang, L. Z. (2016). Effect of Al substitution on the microstructure and lithium storage performance of nickel hydroxide. *J. Power Sources* 307, 114–121. doi: 10.1016/j.jpowsour.2015.12.129
- Li, Y. W., Xu, W. Q., Xie, Z. P., Zhang, L. Z., and Yao, J. H. (2017a). Structure and lithium storage performances of nickel hydroxides synthesized with different nickel salts. *Ionics* 23, 1625–1636. doi: 10.1007/s11581-017-1983-3
- Li, Y. W., Xu, W. Q., Zheng, Y. Y., Yao, J. H., and Xiao, J. R. (2017b). Hierarchical flower-like nickel hydroxide with superior lithium storage performance. *J. Mater. Sci. Mater. Electron.* 28, 17156–17160. doi: 10.1007/s10854-017-7643-6
- Lin, L., and Pan, Q. M. (2015). ZnFe₂O₄/C/graphene nanocomposites as excellent anode materials for lithium batteries. *J. Mater. Chem. A* 3, 1724–1729. doi: 10.1039/C4TA05368K
- Lu, D. B., Zhang, Y., Lin, S. X., Wang, L. T., and Wang, C. M. (2013). Synthesis of magnetic ZnFe₂O₄/graphene composite and its application in photocatalytic degradation of dyes. *J. Alloy Compd.* 579, 336–342. doi: 10.1016/j.jallcom.2013.06.098
- Lu, X. J., Xie, A., Zhang, Y., Zhong, H., Xu, X., Liu, H., et al. (2017). Three dimensional graphene encapsulated ZnO-ZnFe₂O₄ composite hollow microspheres with enhanced lithium storage performance. *Electrochim. Acta* 249, 79–88. doi: 10.1016/j.electacta.2017.08.001

- Massé, R. C., Liu, C., Li, Y., Mai, L., and Cao, G. (2017). Energy storage through intercalation reactions: electrodes for rechargeable batteries. *Natl. Sci. Rev.* 4, 26–53. doi: 10.1093/nsr/nww093
- Nitta, N., and Yushin, G. (2014). High-capacity anode materials for lithium-ion batteries: choice of elements and structures for active particles. *Part Part. Syst. Charact.* 31, 317–336. doi: 10.1002/ppsc.201300231
- NuLi, Y.-N., Chu, Y.-Q., and Qin, Q.-Z. (2004). Nanocrystalline ZnFe₂O₄ and Ag-doped ZnFe₂O₄ films used as new anode materials for Li-ion batteries. *J. Electrochem. Soc.* 151, A1077–A1083. doi: 10.1149/1.1760576
- Pailhé, N., Wattiaux, A., Gaudon, M., and Demourgues, A. (2008). Correlation between structural features and vis-NIR spectra of α-Fe₂O₃ hematite and AFe₂O₄ spinel oxides (A=Mg, Zn). *J. Solid State Chem.* 181, 1040–1047. doi: 10.1016/j.jssc.2008.02.009
- Pan, L., Zhu, X.-D., Xie, X.-M., and Liu, Y.-T. (2015a). Delicate ternary heterostructures achieved by hierarchical co-assembly of Ag and Fe₃O₄ nanoparticles on MoS₂ nanosheets: morphological and compositional synergy in reversible lithium storage. *J. Mater. Chem. A* 3, 2726–2733. doi: 10.1039/C4TA06348A
- Pan, L., Zhu, X.-D., Xie, X.-M., and Liu, Y.-T. (2015b). Smart hybridization of TiO₂ nanorods and Fe₃O₄ nanoparticles with pristine graphene nanosheets: hierarchically nanoengineered ternary heterostructures for high-rate lithium storage. *Adv. Funct. Mater.* 25, 3341–3350. doi: 10.1002/adfm.201404348
- Qiao, L., Wang, X. H., Qiao, L., Sun, X. L., Li, X. W., Zheng, Y. X., et al. (2013). Single electrospun porous NiO-ZnO hybrid nanofibers as anode materials for advanced lithium-ion batteries. *Nanoscale* 57, 3037–3042. doi: 10.1039/c3nr34103h
- Qu, Y., Zhang, D., Wang, X., Qiu, H. L., Zhang, T., Zhang, M., et al. (2017). Porous ZnFe₂O₄ nanospheres as anode materials for Li-ion battery with high performance. *J. Alloy Compd.* 721, 697–704. doi: 10.1016/j.jallcom.2017.06.031
- Rai, A. K., Kim, S., Gim, J., Alfaruqi, M. H., Methew, V., and Kim, J. (2014). Electrochemical lithium storage of a ZnFe₂O₄/graphene nanocomposite as an anode material for rechargeable lithium ion batteries. *RSC Adv.* 4, 47087–47095. doi: 10.1039/C4RA08414D
- Rauda, I. E., Augustyn, V., Dunn, B., and Tolbert, S. H. (2013). Enhancing pseudocapacitive charge storage in polymer templated mesoporous materials. *Acc. Chem. Res.* 46, 1113–1124. doi: 10.1021/ar300167h
- Reddy, M. V., Subba Rao, G. V., and Chowdari, B. V. (2013). Metal oxides and oxyalts as anode materials for Li ion batteries. *Chem. Rev.* 113, 5364–5457. doi: 10.1021/cr3001884
- Scrosati, B., Hassoun, J., and Sun, Y.-K. (2011). Lithium-ion batteries. A look into the future. *Energy Environ. Sci.* 4, 3287–3295. doi: 10.1039/c1ee01388b
- Shi, J. J., Zhou, X. Y., Liu, Y., Su, Q. M., Zhang, J., and Du, G. H. (2015). One-pot solvothermal synthesis of ZnFe₂O₄ nanospheres/graphene composites with improved lithium-storage performance. *Mater. Res. Bull.* 65, 204–209. doi: 10.1016/j.materresbull.2015.01.057
- Sun, H., Xin, G., Hu, T., Yu, M., Shao, D., and Sun, X. (2014). High-rate lithiation-induced reactivation of mesoporous hollow spheres for long-lived lithium-ion batteries. *Nat. Commun.* 5:4526. doi: 10.1038/ncomms5526
- Tang, Y., Zhang, Y., Li, W., Ma, B., and Chen, X. (2015). Rational material design for ultrafast rechargeable lithium-ion batteries. *Chem. Soc. Rev.* 44, 5926–5940. doi: 10.1039/C4CS00442F
- Thankachan, R. M., Rahman, M. M., Sultana, I., Glushenkov, A. M., Thomas, S., Kalarikkal, N., et al. (2015). Enhanced lithium storage in ZnFe₂O₄-C nanocomposite produced by a low-energy ball milling. *J. Power Sources* 282, 462–470. doi: 10.1016/j.jpowsour.2015.02.039
- Wang, C. L., Tan, X., Yan, J. T., Chai, B., Li, J. F., and Chen, S. Z. (2017). Electrospinning direct synthesis of magnetic ZnFe₂O₄/ZnO multi-porous nanotubes with enhanced photocatalytic activity. *Appl. Surf. Sci.* 396, 780–790. doi: 10.1016/j.apsusc.2016.11.029
- Wang, M. Y., Huang, Y., Chen, X. F., Wang, K., Wu, H. W., Zhang, N., et al. (2017). Synthesis of nitrogen and sulfur co-doped graphene supported hollow ZnFe₂O₄ nanosphere composites for application in lithium-ion batteries. *J. Alloy Compd.* 691, 407–415. doi: 10.1016/j.jallcom.2016.08.285
- Wang, S., Xiao, C., Xing, Y., Xu, H., and Zhang, S. (2015). Carbon nanofibers/nanosheets hybrid derived from cornstalks as a sustainable anode for Li-ion batteries. *J. Mater. Chem. A* 3, 6742–6746. doi: 10.1039/C5TA00050E
- Xing, Z., Ju, Z., Yang, J., Xu, H., and Qian, Y. (2012). One-step hydrothermal synthesis of ZnFe₂O₄ nano-octahedrons as a high capacity anode material for Li-ion batteries. *Nano Res.* 5, 477–485. doi: 10.1007/s12274-012-0233-2
- Xu, H., Zhu, X.-D., Sun, K.-N., Liu, Y.-T., and Xie, X.-M. (2015). Elaborately designed hierarchical heterostructures consisting of carbon-coated TiO₂(B) nanosheets decorated with Fe₃O₄ nanoparticles for remarkable synergy in high-rate lithium storage. *Adv. Mater. Interfaces* 2:1500239. doi: 10.1002/admi.201500239
- Yang, T. B., Zhang, W. X., Li, L. L., Jin, B., Jin, E., Jeong, S., et al. (2017). In-situ synthesized ZnFe₂O₄ firmly anchored to the surface of MWCNTs as a long-life anode material with high lithium storage performance. *Appl. Surf. Sci.* 425, 978–987. doi: 10.1016/j.apsusc.2017.07.152
- Yao, J. H., Li, X. H., Pan, L. P., and Mo, J. M. (2012). Enhancing physicochemical properties and indium leachability of indium-bearing zinc ferrite mechanically activated using tumbling mill. *Metall. Mater. Trans. B* 43, 449–459. doi: 10.1007/s11663-012-9641-7
- Yao, J. H., Li, Y. W., Massé, R. C., Uchaker, E., and Cao, G. Z. (2018a). Revitalized interest in vanadium pentoxide as cathode material for lithium-ion batteries and beyond. *Energy Storage Mat.* 11, 205–259. doi: 10.1016/j.ensm.2017.10.014
- Yao, J. H., Li, Y. W., Song, X. B., Zhang, Y. F., and Yan, J. (2018b). Lithium storage performance of zinc ferrite nanoparticle synthesized with the assistance of triblock copolymer P123. *J. Nanosci. Nanotechnol.* 18, 3599–3605. doi: 10.1166/jnn.2018.14684
- Yao, J. H., Zhang, Y. F., Yan, J., Huang, B., Li, Y. W., and Xiao, S. H. (2018c). Nanoparticles-constructed spinel ZnFe₂O₄ anode material with superior lithium storage performance boosted by pseudocapacitance. *Mater. Res. Bull.* 104, 188–193. doi: 10.1016/j.materresbull.2018.04.023
- Yao, L., Hou, X. H., Hu, S. J., Tang, X. Q., Liu, X., and Ru, Q. (2014a). An excellent performance anode of ZnFe₂O₄/flake graphite composite for lithium ion battery. *J. Alloy Compd.* 585, 398–403. doi: 10.1016/j.jallcom.2013.09.066
- Yao, L., Hou, X. H., Hu, S. J., Wang, J., Li, M., Su, C., et al. (2014b). Green synthesis of mesoporous ZnFe₂O₄/C composite microspheres as superior anode materials for lithium-ion batteries. *J. Power Sources* 258, 305–313. doi: 10.1016/j.jpowsour.2014.02.055
- Yao, X., Kong, J. H., Zhou, D., Zhao, C. Y., Zhou, R., and Liu, X. H. (2014c). Mesoporous zinc ferrite/graphene composites: Towards ultra-fast and stable anode for lithium-ion batteries. *Carbon* 79, 493–499. doi: 10.1016/j.carbon.2014.08.007
- Yi, T.-F., Mei, J., and Zhu, Y.-R. (2016). Key strategies for enhancing the cycling stability and rate capacity of LiNi_{0.5}Mn_{1.5}O₄ as high-voltage cathode materials for high power lithium-ion batteries. *J. Power Sources* 316, 85–105. doi: 10.1016/j.jpowsour.2016.03.070
- Yi, T.-F., Yang, S.-Y., and Xie, Y. (2015). Recent advances of Li₄Ti₅O₁₂ as a promising next generation anode material for high power lithium-ion batteries. *J. Mater. Chem. A* 3, 5750–5777. doi: 10.1039/C4TA06882C
- Yu, S. J., Ng, V. M. H., Wang, F. J., Xiao, Z. H., Li, C. Y., Kong, L. B., et al. (2018). Synthesis and application of iron-based nanomaterials as anodes of lithium-ion batteries and supercapacitors. *J. Mater. Chem. A* 6, 9332–9367. doi: 10.1039/C8TA01683F
- Yuan, C., Wu, H. B., Xie, Y., and Lou, X. W. (2014). Mixed transition-metal oxides: design, synthesis, and energy-related applications. *Angew. Chem. Int. Ed.* 53, 1488–1504. doi: 10.1002/anie.201303971
- Yue, H., Wang, Q. X., Shi, Z. P., Ma, C., Ding, Y. M., Huo, N. N., et al. (2015). Porous hierarchical nitrogen-doped carbon coated ZnFe₂O₄ composites as high performance anode materials for lithium ion batteries. *Electrochim. Acta* 180, 622–628. doi: 10.1016/j.electacta.2015.08.139
- Zhang, L., Wu, H. B., and Lou, X. W. (2014). Iron-oxide-based advanced anode materials for lithium-ion batteries. *Adv. Energy Mater.* 4:1300958. doi: 10.1002/aenm.201300958
- Zhang, L. H., Wei, T., Yue, J. M., Sheng, L. Z., Jiang, Z. M., Yang, D. R., et al. (2017). Ultra-small and highly crystallized ZnFe₂O₄ nanoparticles within double graphene networks for super-long life lithium-ion batteries. *J. Mater. Chem. A* 5, 11188–11196. doi: 10.1039/C7TA02726E
- Zhang, Q., Chen, H. X., Luo, L. L., Zhao, B., Luo, H., Han, X., et al. (2018). Harnessing the concurrent reaction dynamics in active Si and Ge to achieve high performance of lithium-ion batteries. *Energy Environ. Sci.* 11, 669–681. doi: 10.1039/C8EE00239H

- Zhang, Q., Uchaker, E., Candelaria, S. L., and Cao, G. (2013). Nanomaterials for energy conversion and storage. *Chem. Soc. Rev.* 42, 3127–3171. doi: 10.1039/c3cs00009e
- Zhang, S. L., Zhao, K. J., Zhu, T., and Li, J. (2017). Electrochemomechanical degradation of high-capacity battery electrode materials. *Prog. Mater. Sci.* 89, 479–521. doi: 10.1016/j.pmatsci.2017.04.014
- Zhang, Y. M., Pelliccione, C. J., Brady, A. B., Guo, H. Y., Smith, P. F., Liu, P., et al. (2017). Probing the Li insertion mechanism of ZnFe₂O₄ in Li-ion batteries: a combined X-ray diffraction, extended X-ray absorption fine structure, and density functional theory study. *Chem. Mater.* 29, 4282–4292. doi: 10.1021/acs.chemmater.7b00467
- Zhao, D., Xiao, Y., Wang, X., Gao, Q., and Cao, M. H. (2014). Ultra-high lithium storage capacity achieved by porous ZnFe₂O₄/α-Fe₂O₃ micro-octahedrons. *Nano Energy* 7, 124–133. doi: 10.1016/j.nanoen.2014.05.001
- Zheng, Y., Zhou, T., Zhang, C., Mao, J., Liu, H., and Guo, Z. (2016). Boosted charge transfer in SnS/SnO₂ heterostructures: toward high rate capability for sodium-ion batteries. *Angew. Chem.* 128, 3469–3474. doi: 10.1002/ange.201510978
- Zheng, Y. Y., Li, Y. W., Yao, J. H., Huang, Y., and Xiao, S. H. (2018). Facile synthesis of porous tubular NiO with considerable pseudocapacitance as high capacity and long life anode for lithium-ion batteries. *Ceram. Int.* 44, 2568–2577. doi: 10.1016/j.ceramint.2017.11.017
- Zheng, Z. M., Zao, Y., Zhang, Q. B., Cheng, Y., Chen, H. X., Zhang, K. L., et al. (2018). Robust erythrocyte-like Fe₂O₃@carbon with yolk-shell structures as high-performance anode for lithium ion batteries. *Chem. Eng. J.* 347, 563–573. doi: 10.1016/j.cej.2018.04.119
- Zhou, D., Jia, H. P., Rana, J., Placke, T., Scherb, T., Kloepsch, R., et al. (2017). Local structural changes of nano-crystalline ZnFe₂O₄ during lithiation and de-lithiation studied by X-ray absorption spectroscopy. *Electrochim. Acta* 246, 699–706. doi: 10.1016/j.electacta.2017.06.098
- Zhu, X. D., Wang, K. X., Yan, D. J., Le, S. R., Ma, R. J., Sun, K. N., et al. (2015). Creating a synergistic interplay between tubular MoS₂ and particulate Fe₃O₄ for improved lithium storage. *Chem. Commun.* 51, 11888–11891. doi: 10.1039/C5CC03898G
- Zhu, Y.-R., and Yi, T.-F. (2016). Recent progress in the electrolytes for improving the cycling stability of LiNi_{0.5}Mn_{1.5}O₄ high-voltage cathode. *Ionics*, 22, 1759–1774. doi: 10.1007/s11581-016-1788-9

Conflict of Interest Statement: The authors declare that the research was conducted in the absence of any commercial or financial relationships that could be construed as a potential conflict of interest.

Copyright © 2018 Yao, Yan, Huang, Li, Xiao and Xiao. This is an open-access article distributed under the terms of the Creative Commons Attribution License (CC BY). The use, distribution or reproduction in other forums is permitted, provided the original author(s) and the copyright owner(s) are credited and that the original publication in this journal is cited, in accordance with accepted academic practice. No use, distribution or reproduction is permitted which does not comply with these terms.